HHS Public Access

Author manuscript

Nat Chem Biol. Author manuscript; available in PMC 2017 April 17.

Published in final edited form as:

Nat Chem Biol. 2016 December ; 12(12): 1023–1030. doi:10.1038/nchembio.2194.

Oligosaccharyltransferase Inhibition Induces Senescence in RTK-Driven Tumor Cells

Cecilia Lopez-Sambrooks[1], **Shiteshu Shrimal**[2], **Carol Khodier**[3], **Daniel P. Flaherty**[4], **Natalie Rinis**[1], **Jonathan C. Charest**[1], **Ningguo Gao**[5], **Peng Zhao**[6], **Lance Wells**[6], **Timothy A. Lewis**[3], **Mark A. Lehrman**[5], **Reid Gilmore**[2], **Jennifer E. Golden**[4,8], and **Joseph N. Contessa**[1,7,*]

[1]Department of Therapeutic Radiology, Yale School of Medicine, New Haven, CT 06511

[2]Department of Biochemistry and Molecular Pharmacology, University of Massachusetts Medical School, Worcester, MA 01605

[3]Center for the Science of Therapeutics, Broad Institute of MIT and Harvard, Cambridge, MA 02142

[4]University of Kansas Specialized Chemistry Center, University of Kansas, Lawrence, Kansas 66047

[5]Department of Pharmacology, UT Southwestern Medical Center at Dallas, 6001 Forest Park Rd. Dallas, TX 75390

[6]Complex Carbohydrate Research Center, Department of Biochemistry and Molecular Biology, University of Georgia, Athens, GA 30602

[7]Department of Pharmacology, Yale School of Medicine, New Haven, CT 06511

Abstract

Asparagine (N)-linked glycosylation is a protein modification critical for glycoprotein folding, stability, and cellular localization. To identify small molecules that inhibit new targets in this biosynthetic pathway, we initiated a cell-based high throughput screen and lead compound optimization campaign that delivered a cell permeable inhibitor (NGI-1). NGI-1 targets the oligosaccharyltransferase (OST), a hetero-oligomeric enzyme that exists in multiple isoforms and transfers oligosaccharides to recipient proteins. In non-small cell lung cancer cells NGI-1 blocks cell surface localization and signaling of the EGFR glycoprotein, but selectively arrests proliferation in only those cell lines that are dependent on EGFR (or FGFR) for survival. In these cell lines OST inhibition causes cell cycle arrest accompanied by induction of p21,

*To whom correspondence may be addressed: joseph.contessa@yale.edu.

[8]Current address: School of Pharmacy, University of Wisconsin, Madison, Wisconsin 53705-2222.

AUTHOR CONTRIBUTIONS:

C.L.S. designed and performed the cell biology experiments in NSCLC cells and contributed to analysis and interpretation of all presented data. N.R. performed and analyzed the CTSA assays; J.C.C. performed experiments in CHO and Lec cells. J.N.C designed the study and was involved in all experimental designs, data analysis, and data interpretation. S.S. and R.G. designed and performed in vitro glycosylation studies. C.K. and T.A.L. performed and triaged the HTS; D.P.F. and J.E. G. performed analysis of SAR and synthesis of chemical analogs; N.G. and M.A.L. performed the LLO analysis; P.Z and L.W. performed the MS data. All authors contributed to writing the manuscript.

Competing financial interests: Dr. Contessa and Dr. Golden are listed as Inventors on a provisional patent application for the analogs reported in this manuscript.

autofluorescence, and changes in cell morphology; all hallmarks of senescence. These results identify OST inhibition as a potential therapeutic approach for treating receptor tyrosine kinase-dependent tumors and provides a chemical probe for reversibly regulating N-linked glycosylation in mammalian cells.

INTRODUCTION

Asparagine (N)-linked glycosylation is a co- and post-translational modification common to proteins of the endoplasmic reticulum (ER) and secretory pathway[1]. This process requires the biosynthesis of a glycan precursor, or lipid linked oligosaccharide (LLO), and involves the coordinated function of at least 30 gene products and 17 enzymatic activities[2,3]. LLO synthesis is initiated in the cytosol through addition of N-acetylglucosamine to phosphorylated dolichol, an enzymatic step that is blocked by the natural product tunicamycin[4] (see Supplementary Results, Supplementary Fig. 1 for a pathway overview). Sequential carbohydrate addition by glycosyltransferases associated with the cytosolic ER leaflet elongate the LLO. The resulting dolichol-linked $Man_5GlcNAc_2$ intermediate is then transferred into the lumen of the ER by a poorly understood mechanism[5–7]. Proteins that synthesize and transport carbohydrate precursors, along with glycosyltransferases of the ER lumen, add mannosyl and glucosyl residues to form the $Glc_3Man_9GlcNAc_2$ LLO. This mature glycan is then transferred to NXT/S (where X cannot be P) consensus sequons of nascent proteins by the oligosaccharyltransferase (OST) enzyme complex[8–10].

Although the biochemical basis for synthesis and transfer of N-linked glycans to recipient proteins has been largely elucidated, control of this process by mammalian cells is not well understood. N-linked glycosylation was initially considered to be constitutive without sites of regulation. This belief was based on two fundamental observations: (1) that many of the N-linked glycosylation genes are essential and (2) the prevalent use of tunicamycin which induces cell death. This concept, however, was incongruent with discoveries about the biology of the OST. Yeast genetics demonstrated that several of the OST subunits were in fact non-essential, requiring synthetic lethal strategies for identification[11–13]. Furthermore the single yeast OST catalytic subunit (STT3) was found to be encoded by two separate homologues in mammals, STT3A and STT3B, suggesting a mechanism for regulation of LLO transfer[14,15]. The hetero-oligomeric mammalian OST complexes are composed of a single copy of a catalytic subunit (either STT3A or STT3B), a shared set of at least five non-catalytic subunits, plus catalytic subunit specific auxiliary subunits yielding multiple isoforms[16–18]. Thus the OST represents at least one enzymatic node for control of N-linked glycosylation and provides molecular evidence for a model where N-linked glycosylation itself can be actively regulated.

Another challenge for the field of glycobiology is the difficulty in attributing the consequences of abnormal N-glycan transfer in the ER to the altered function of specific glycoproteins. For example human congenital disorders of glycosylation have disparate clinical presentations and it has been difficult to identify either the specific proteins or the cellular contexts that are most sensitive to disruption of glycosylation[19]. It has been suggested by our group and others[20–22] that receptor tyrosine kinase (RTK) glycoproteins

such as epidermal growth factor receptor (EGFR) and fibroblast growth factor receptor (FGFR) family members are sensitive to perturbations in N-glycosylation, and thus RTKs may mediate the effects of abnormal N-linked glycosylation. These receptors are the subject of intense study in oncology and have been identified in tumor subpopulations as drivers of 'oncogene addiction', a cellular state where inhibition of the oncogene's function also eliminates activity of the principal signaling pathways for proliferation[23]. Thus understanding the interplay between N-linked glycosylation and RTK function should provide new mechanistic insights on cellular sensitivity to glycosylation defects as well as identify novel approaches for targeted inhibition of RTK function.

The study of N-linked glycosylation in living cells would be significantly improved by the generation of chemical probes that disrupt the function of this biosynthetic pathway. Although peptidomimetics that block N-linked glycosylation have been developed[24,25], cell permeability for these inhibitors remains a challenge. We therefore developed a tiered high throughput screening (HTS) methodology to identify small molecule inhibitors of protein N-linked glycosylation. In the present study we report results from a screen of 358,301 compounds, subsequent establishment of chemical structure activity relationships, and characterization of the biological target. We also investigate the effects of our newly discovered inhibitor in non-small cell lung cancer (NSCLC) cells to identify differential outcomes that are dependent upon cellular contexts of RTK signaling.

RESULTS

HTS for Inhibitors of N-linked Glycosylation

A HTS of 358,301 compounds from the National Institutes of Health Molecular Libraries Small Molecule Repository (MLSMR) was performed using a gain of function, cell-based assay for N-linked glycan site occupancy[20,26]. An overview of the HTS strategy including primary, secondary, and tertiary screening is presented in supplementary Figure 2. The primary screen was performed in duplicate and values were normalized to the average of positive control wells (tunicamycin) minus averaged vehicle treated wells per run. Compounds with replicate activity greater than three standard deviations above the mean average of control wells were selected for further study. A subset of 1,845 compounds met this criterion, and were advanced to simultaneous retesting in both the primary screen and a secondary (false positive) cell-based screen. A subset of 730 compounds were further advanced after demonstration of a 40% activating concentration (AC_{40}) less than 10 μM and no activity in the secondary screen. Compounds were further triaged from consideration by consulting the Pubchem bioassay database and deprioritizing compounds showing a promiscuity rate higher than 5% across assays or by removing PAINS scaffolds[27]. Remaining compounds were assessed by medicinal chemistry review to score synthetic tractability and predicted issues with instability, poor solubility, or toxicity. This analysis yielded 39 compounds that were tested in a cell-free assay to detect luciferase inhibitors[26,28] and by western blot analysis to detect gel mobility changes of the luciferase reporter consistent with inhibition of N-linked glycosylation. This approach identified one aminobenzamidosulfonamide compound that blocked N-linked glycosylation.

To better understand the connection between structure and activity, analogs were prepared and tested in the D54-ERLucT cell based assay for inhibition of N-linked glycosylation (Fig. 1a). The assay was used to estimate and compare AC_{40} values and guide the design of additional compounds. This effort generated 36 unique compounds with modifications to the amine component of the sulfonamide functionality (red), the pyrrolidine moiety (blue) or the methylaminothiazole group (green; supplementary Note). Generally, incorporation of larger sulfonamides (*i.e.*, larger secondary amines appended to the sulphone) was not well tolerated, resulting in erosion of potency (7 analogs). However, steric interactions could be mitigated by the introduction of a hydrogen bond accepting oxygen in a larger cyclic amine. Thus, morpholine was determined to be an acceptable surrogate for the dimethylamine component of the sulfonamide (Fig. 1a). The pyrrolidine group (blue) was replaced with various alkyl, cycloalkyl, and amine groups (7 compounds). The aminothiazole moiety was derivatized most extensively of all three regions (green highlighted area, 22 analogs). Elaboration or simplification of the thiazole itself was permitted, though any attempt to replace the thiazole with another heterocycle or substituted phenyl ring was inferior in terms of potency. The activity for all analogs is reported in supplementary Tables 1, 2 and 3. Analogs were also tested for toxicity in HepG2 and HEK293 cells using the Celltiter Glo viability assay after 72 h of compound exposure, and all analogs showed no cell toxicity liability (EC_{50} > 30 μM; suppl. Table 1–3). Analogs with the highest potency in the luciferase assay were retested with western blot analysis to ensure that measurements of luciferase activation corresponded to loss of N-linked glycosylation.

These efforts revealed a small molecule chemical probe with N-linked glycosylation inhibitory activity that lacked cell toxicity and we designate as N-linked Glycosylation Inhibitor-1 (NGI-1). Using dose response data for luciferase activity the AC_{50} (equivalent to IC_{50}) of NGI-1 in intact D54 ER-LucT cells in culture was estimated to be 1.1 μM (Fig. 1b). Western blot analysis of NGI-1 treated cell cultures also demonstrated dose response loss of luciferase N-linked glycosylation that directly corresponds to the ~1 μM in vitro IC_{50} (Fig. 1c; suppl. Fig 9). Notably, unlike tunicamycin, NGI-1 did not completely abolish all N-linked glycosylation even at doses that were 25 times the estimated IC_{50}. This distinctive inhibitory pattern suggested that NGI-1 has a different mechanism of action and likely a different cellular target from that of tunicamycin.

NGI-1 disrupts oligosaccharyltransferase function

To delimit the potential targets of NGI-1 we used glycosylation defective CHO Lec15[29] and Lec35[30] cells which have loss of DPM2 and MPDU1 function, respectively (suppl. Fig. 1), and synthesize truncated $Man_5GlcNAc_2$ LLOs. Stable cell lines expressing the ER-LucT were generated in both Lec15 and Lec35 to test the effect of NGI-1 and tunicamycin on N-linked glycosylation. DPAGT1 (Dolichyl-phosphate N-Acetylglucosamine phosphotransferase 1), the target of tunicamycin, is active and tunicamycin-responsive in both cell lines (Fig. 2a; suppl. Fig. 9b). Similar to tunicamycin, NGI-1 caused instability of the luciferase reporter, indicating that the NGI-1 target was present in both cell lines. This data suggested that the target of NGI-1 is required for either synthesis of the $Man_5GlcNAc_2$ LLO species or for its transfer to the target protein (but not for extension of $Man_5GlcNAc_2$ to $Glc_3Man_5GlcNAc_2$). To differentiate between these possibilities fluorophore assisted

carbohydrate electrophoresis (FACE) analysis was performed to determine the effect of NGI-1 on LLO synthesis (Fig. 2b). Tunicamycin was used as a positive control and blocked all LLO production, consistent with inhibition of the enzyme that catalyzes the first committed step in LLO synthesis. In contrast NGI-1 did not impair LLO synthesis, and actually increased $Glc_3Man_9GlcNAc_2$ LLO by 31% ($p < .01$), suggesting that NGI-1 did not abrogate LLO synthesis but instead reduced LLO consumption. Coupled with decreased protein glycosylation, these results suggested that NGI-1 blocks the transfer of LLOs to recipient glycoproteins.

The OST is an ER resident, multi-subunit enzymatic complex that transfers oligosaccharides from LLO donors to acceptor protein sequons[31]. At a lesser rate the OST also cleaves LLOs and releases oligosaccharides as free glycans in the ER lumen. Both enzymatic products of OST, free glycans and N-glycans, were therefore analyzed with and without NGI-1 treatment using streptolysin-O permeabilized CHO cells to facilitate access of OST substrate tripeptides (Fig. 2c). Addition of a control peptide without the N-linked glycosylation consensus sequence (QYT) led to readily detectable levels of free glycans (left panel), while addition of an acceptor peptide containing the consensus sequence (NYT) followed by PNGase treatment led to detection of glycans cleaved from N-linked glycopeptides (right panel). Since N-glycosylation and LLO hydrolysis are competing reactions of OST, the presence of NYT peptide reduced the production of free glycans. Using this experimental design NGI-1 was shown to substantially reduce the production of both OST products (free glycans and N-glycans), providing biochemical evidence that OST is the target of NGI-1. To isolate the activity of the OST, canine pancreas microsomes were used with *in vitro* translation of prosaposin (pSAP) mRNA to provide high concentrations of endogenous LLO substrate, OST enzyme, and a glycoprotein acceptor in a cell free system[32]. NGI-1 showed a dose dependent inhibition of pSAP N-linked glycosylation (Fig. 3a), demonstrating independence from *de novo* synthesis of LLOs, proteins, or other cellular factors and consistent with OST inhibition.

Mammalian genomes encode two isoforms of the OST catalytic subunit; STT3A and STT3B. Knockdown of each subunit has been shown to have specific effects on discrete N-linked glycosylation sites[15,33]. For example, pSAP is known to have five sites that are blocked by STT3A knockdown alone, and sex hormone binding globulin (SHBG) is known to have two sites that are blocked by STT3B knockdown alone. Metabolic pulse labeling of pSAP and SHBG in HeLa cells shows that NGI-1 blocks both STT3A and STT3B dependent glycosylation sites (Fig. 3b). Furthermore, inhibition of site occupancy for both isoform specific sites is reversible, as omission of NGI-1 during the pulse labeling interval (20 minutes) restored N-linked glycosylation (Fig. 3c).

Although NGI-1 reduces glycosylation of both STT3A and STT3B dependent sites, the effect of NGI-1 on STT3A dependent sites appeared incomplete (Fig. 3b). Dose response analysis confirmed that while NGI-1 completely blocks LLO transfer to STT3B dependent sites (SHBG), it is less potent and incompletely blocks glycosylation of STT3A dependent sites (pSAP; Fig. 3d, suppl. Fig. 3a). This data suggests differential effects on OST complexes containing either the STT3A or STT3B catalytic subunit. To examine the interaction of NGI-1 with OST subunits, cellular thermal shift assays (CETSA) were

performed[34]. The results showed that NGI-1 stabilizes STT3B (Fig. 3e; suppl. Fig. 3b, 9c, 9k), shifting the melting curve of the protein and providing direct evidence of target engagement. NGI-1 did not stabilize STT3A in this analysis, consistent with its partial effect on STT3A dependent glycosylation. Taken together these results provide strong evidence that NGI-1 is a reversible catalytic subunit inhibitor of the OST that has higher specificity for STT3B compared to STT3A.

NGI-1 blocks EGFR glycosylation and cell surface transport

The EGFR is a highly glycosylated transmembrane RTK protein with eleven consensus N-linked glycosylation sites in the extracellular domain. This cell surface growth factor receptor has been identified as a key driver of proliferation and survival signaling in malignant tumors, and we therefore sought to investigate the consequences of NGI-1 mediated OST inhibition on EGFR function. NGI-1 blocked EGFR N-linked glycosylation in lung adenocarcinoma cells as assessed by decreased molecular weight on SDS-PAGE (Fig. 4a; suppl. Fig. 9d). However, residual glycosylation was also indicated by gel mobility differences from that of PNGase treated controls or from samples where LLO synthesis was blocked with tunicamycin. This mobility difference was abolished by digestion of NGI-1 treated samples with PNGase, confirming that NGI-1 treatment blocks the transfer of most, but not all, N-linked glycans to the EGFR.

N-linked glycosylation is a critical step for the quality control and trafficking of transmembrane glycoproteins like the EGFR. To determine the effect of NGI-1 on EGFR distribution within the cell, membrane impermeable biotin labeling of intact cells followed by streptavidin precipitation was performed (Fig. 4b; suppl. Fig. 9e). In controls EGFR was biotinylated, consistent with its plasma membrane expression, but in NGI-1 treated cells the EGFR was predominantly found in the non-biotinylated intracellular fraction suggesting a change in cellular localization. Confocal microscopy of EGFR (red) and the ER-resident protein calreticulin (CRT; green) was then undertaken in H3255 lung adenocarcinoma cells to define the effect of NGI-1 on EGFR localization (Fig. 4c). In controls EGFR immunofluorescence was discretely localized to the plasma membrane, however, 24 h of NGI-1 treatment caused a dramatic shift of the EGFR to an intracellular compartment without altering the cellular localization of CRT. Colocalization of EGFR and CRT was then quantified using Image J Colormap Software (Fig. 4d) and showed a significantly increased positive correlation for signal association ($p<.05$). Identical results were observed for the HCC-827 NSCLC line (suppl. Fig. 4; suppl. Fig. 4e). Together these results suggest that OST inhibition with NGI-1 blocks EGFR trafficking to the cell surface, and that hypo-glycosylated receptors are retained in the ER and secretory pathway.

A glycoproteomic analysis was also performed to screen for differential effects of NGI-1 on glycoprotein glycosylation and localization. This approach identified 16 partially glycosylated proteins expressed at the cell surface, several of which were integrins, and contained both NGI-1 sensitive and insensitive glycosylation sites (suppl. Table 4). To confirm this result, the effect of NGI-1 on Integrin B1 (ITB1) glycosylation and localization was further examined. NGI-1 treatment significantly reduced ITB1 glycosylation after extended treatment (48 h; Fig. 4e; suppl. Fig. 9f), but unlike the EGFR, hypo- glycosylated

ITB1 was found in the cell surface biotinylated fraction and also visualized at the cell surface with confocal microscopy (Fig. 4f). These results demonstrate differential effects of NGI-1 on individual proteins and imply that NGI-1 does not generally block the transport of cell surface receptors through the secretory pathway but rather alters trafficking of specific proteins.

NGI-1 blocks proliferation of RTK dependent NSCLC

Mutation of the EGFR kinase domain (KD) is present in approximately 10% of lung adenocarcinomas in western populations[35,36]. This mutation increases EGFR tyrosine kinase activity, drives tumorigenesis, and produces tumors that are dependent, or 'addicted', to RTK signaling for proliferation[37]. Because NGI-1 reduces EGFR glycosylation and localization, the effects of this inhibitor on EGFR-dependent signaling were also examined. NGI-1 blocked phosphorylation of KD mutant EGFR in PC9 cells after treatment for 1 day (Fig. 5a; suppl. Fig. 9g)), and after 3 days reduced subsequent cell proliferation by more than 90% in MTT assays ($p < .001$; Fig. 5b). In contrast the A549 cell line, which harbors a downstream activating KRAS mutation (G12S), continued to proliferate after NGI-1 exposure (Fig. 5c) despite effective blockade of EGFR glycosylation (Fig 5a). H3225 and HCC-827, two additional cell lines with EGFR KD mutations, were also found to be sensitive to NGI-1 treatment (suppl. Fig. 5a,b), demonstrating the sensitivity of this phenotype to NGI-1 treatment. Importantly the results with NGI-1 are in contrast to those obtained with tunicamycin which immediately blocks proliferation in both cell lines (Fig 5b,c).

To assess the effects of NGI-1 on cellular signaling, phospho-protein levels of 43 signaling proteins were determined on arrays (Fig. 5d, suppl. Fig. 6a) and are quantified in supplementary Figure 6b. Inhibition of EGFR activation by NGI-1 globally reduced phosphorylation of both kinases and effectors of downstream proliferative signaling in PC9 cells, however, only subtle quantitative effects on these phospho-proteins were observed in A549 cells (Fig. 5d; suppl. Fig. 6b). Significant reductions in phosphorylation of EGFR (Y1068; B2), Akt (T308; B6), p70 S6K (T421/424; D6), Src (Y419; D1), and CREB (S133; C2) suggests that NGI-1 effectively blocks oncogenic signaling from this transmembrane glycoprotein, but has only a minor effect on oncogenic signaling in other cell contexts such as the A549 cells.

The effects of NGI-1 were then compared in two additional lung cancer cell lines; H1581 and H2444. Both of these cell lines are characterized by FGFR amplification, but only H1581 are FGFR1-dependent and sensitive to inhibition with FGFR specific tyrosine kinase inhibitors[38]. NGI-1 treatment enhanced FGFR mobility on PAGE, consistent with inhibition of N-linked glycosylation, and also blocked FGFR1 phosphorylation (Fig. 5e; suppl. Fig. 9h). The multiple bands on western blot represent glycoforms of alternative splice products in the third immunoglobulin domain. Consistent with dependence on FGFR signaling, NGI-1 blocked proliferation of the H1581 cell line but not that of H2444 cells (Fig. 5f,g). Together these results show that NGI-1 has potent inhibitory effects on cell types where proliferative signaling is driven by RTK glycoproteins.

NGI-1 induces senescence in RTK dependent lung cancer

To determine the underlying mechanism for the proliferative changes in RTK driven lung cancer cells after inhibition of N-linked glycosylation with NGI-1, cell cycle and apoptosis were assessed in the PC9 and A549 cell lines. Treatment of both NSCLC cell lines with NGI-1 for 2 or 5 days did not induce apoptosis, though apoptosis was activated by tunicamycin treatment in both cell lines (suppl. Fig. 7a,b). NGI-1 also induced a similar ER stress response in both cell lines indicated by induction of GRP78/BiP protein expression (suppl. Fig. 7c; suppl. Fig. 9l). Analysis of cell cycle distribution by flow cytometry demonstrated a significant increase in G1 for NGI-1 treated PC9 (65% vs 90% $p<.01$; Fig. 6a; suppl. Fig. 8a), H3225 (55% vs 80% $p<.05$; suppl. Fig. 8c) and HCC-827 (50% vs 75% $p<.01$; suppl Fig. 8d) cells after 24 h, but did not significantly change the cell cycle distribution of A549 cells (Fig. 6b; suppl. Fig. 8b). A G1 arrest was also seen after NGI-1 treatment in H1581 cells (55% vs 80% $p<.05$) but not in H2444 cells (suppl. Fig. 8 e,f). Additionally, a sub-G1 peak, which can be observed with induction of apoptosis, was not present in NGI-1 treated PC9 cells, providing further evidence that these cells do not undergo apoptosis. Consistent with the observed G1 cell cycle arrest in PC9 cells, cyclin D1 was reduced at both the mRNA (40% ± 15%, $p<.01$) and protein levels in PC9 cells, but not significantly affected in A549 cells (Fig. 6c,d; suppl. Fig. 9i).

Protein levels of p21 were also analysed in PC9 cells and found to increase within 24 h after NGI-1 treatment (Fig. 6e; suppl. Fig. 9j). This protein is a cell cycle regulator and marker for senescence, raising the possibility that inhibition of N-linked glycosylation with NGI-1 could preferentially induce senescence. We therefore assessed for additional hallmarks of senescence in PC9 and A549 NSCLC cells following control or NGI-1 treatment for 5 days (Fig. 6f,g). In PC9 cells we found increased autofluorescence by flow cytometry (60.4% ± 7.5%, $p<.05$), fluorescent aggregates consistent with lipofuscin accumulation by microscopy, and cell morphology changes characterized by enlarged and flattened cells (Fig. 6f). In comparison none of these changes were detected in A549 cells (Fig. 6g). Together these results provide strong evidence that inhibition of N-linked glycosylation induces cell cycle arrest and senescence in tumor cells with RTK driven oncogenic signaling.

DISCUSSION

In this work we report the results of a successful HTS campaign and the identification of an aminobenzamidosulfonamide chemical series that blocks N-linked glycosylation. NGI-1, the lead compound from this series, alters the enzymatic reaction of glycosylation *per se*, causing a marked reduction of protein N-linked glycosylation and accumulation of lipid linked glycan precursors. NGI-1 reduces N-linked glycosylation through a direct and reversible interaction with the catalytic subunit of the OST. However, because mammalian cells encode two mutually exclusive OST catalytic subunits (STT3A and STT3B), and NGI-1 only partially blocks the STT3A subunit, the overall effect of NGI-1 is incomplete inhibition of glycosylation.

The incomplete inhibition of N-linked glycosylation provides a reasonable explanation for the reduced cellular toxicity of NGI-1 compared to the nucleoside antibiotic, tunicamycin. Tunicamycin completely blocks enzymatic activity of DPAGT1 and eliminates the

production of all lipid linked glycan precursors and all N-linked glycosylation, leading to apoptosis and cell death in virtually all cell types. The diminished effects of NGI-1 are therefore more similar to the aberrant glycosylation seen in congenital disorders of glycosylation (CDG), a group of diseases with reduced N-linked glycosylation efficiency that are most often caused by hypomorphic alleles of enzymes required for glycosylation. CDGs and animal models of these diseases are characterized by a range of developmental abnormalities, but these enzymatic deficiencies may have only subtle effects after embryonic development is complete[39].

In NSCLC cells, we found that NGI-1 has its greatest effects on tumor phenotypes that are dependent, or 'addicted', to RTK glycoproteins. RTK extracellular domains are highly glycosylated, and N-linked glycans contribute to the stable receptor conformations that facilitate cell surface expression, ligand binding, and regulation of downstream signal transduction[21]. We show that proliferation of RTK-dependent NSCLC tumor cells is blocked (PC9, HCC-827, H3255, H1581) while proliferation of other NSCLC cells without RTK driven signaling is NGI-1 insensitive (A549, H2444). In agreement with this data, and despite the observation that RTK glycosylation was reduced in all cell lines, the inhibitory effects of NGI-1 on downstream signaling proteins that regulate proliferation[40–42] were only pronounced in RTK-dependent lines. Finally, NGI-1 also caused a G1 arrest and the appearance of several hallmarks of senescence in only the RTK-dependent NSCLC lines. Together this data argues that RTK driven cell signaling is particularly sensitive to OST inhibition with NGI-1. However, although standard profiling for off-target effects[43] was negative (suppl. Table 5), the possibility that NGI-1 has other cellular targets cannot be definitively excluded at this time. Nevertheless, the sensitivity of RTK dependent tumor phenotypes to NGI-1 treatment suggests that strategies to target N-linked glycosylation could prove useful as a therapeutic approach for treating RTK driven malignancies.

In summary, we introduce a new potent and cell permeable small molecule inhibitor of N-linked glycosylation. NGI-1 has a unique biologic activity; it blocks the transfer of mature glycan precursors to recipient proteins. NGI-1 and its analogs also display reduced cellular toxicity compared to tunicamycin and thus in addition to providing a new chemical probe for advancing basic science research in glycobiology, they may also enable new biotechnology approaches for regulating protein N-linked glycosylation in mammalian cells.

ONLINE METHODS

Cell lines and culture conditions

The H3255, H1581, H2444, HEK293T, and HepG2 cell lines were purchased from the ATCC (Rockville, MD). The PC9 cell line was a gift from Katie Politi, the A549 cell line was a gift from Abhi Patel (both Yale University, New Haven CT), and the HCC-827 line was a gift from Jeff Engelman (MGH, Boston Mass). Glycosylation defective CHO Lec15[29] and Lec35[30] cells which have loss of DPM2 (dolichyl-phosphate mannosyltransferase-2) and MPDU1 (Mannose-P-Dolichol Utilization Defect 1) function have been previously described. Cells were maintained in RPMI media supplemented with 10% FBS and pen/strep at 37 °C in a humidified incubator with 5% CO_2.

High Throughput Screening

The HTS approach using the bioluminescent N-linked glycosylation reporter in D54-ERLucT and D54-LucT cells has been previously described[26]. Briefly, the primary cell-based screen detects N-linked glycan site occupancy using a modified and ER translated luciferase protein with three N-linked glycosylation consensus sequons. Inhibition of glycosylation in D54-ERLucT restores and increases luciferase activity over controls whereas it does not increase activity in the non-ER translated D54-LucT cell line. The methodology for the primary (D54-ERlucT), secondary false positive (D54-LucT), and tertiary (luciferase inhibition) screens as well as toxicity assays with CellTitre Glo are deposited in Pubchem (AID 588693). Genedata Screener software with the Smartfit algorithm was used for to generate AC_{40} values for comparative analysis of analogs.

LLO, Protein, and RNA Detection

Fluorophore assisted carbohydrate electrophoresis (FACE) was performed as previously described[44,45]. Control (Ac-Gln-Tyr-Thr-CONH2) and acceptor (Ac-Asn-Tyr-Thr-CONH2) peptides were used for permeabilized cell experiments. Metabolic labeling of HeLa cells, transfection of prosaposin (pSAP) and sex hormone binding globulin (SHBG) vectors, and knockdown of STT3A and STT3B to monitor N-linked glycosylation knockdown were performed as described[33]. Cellular Thermal Shift Assays (CETSA) were performed as described[34]. Briefly, cells were treated with 100 μM NGI-1 for 30 min and then harvested and resuspended in complete DMEM medium supplemented with 100 μM NGI-1. Resuspended cells were subjected to thermal treatment for 3 min, lysed, and the soluble protein fraction was analyzed by western blot. Western blot analysis was performed as previously described[26]. The following primary antibodies were used: rabbit anti-STT3B (Proteintech; 1:1000), rabbit anti-STT3A (Proteintech; 1:1000), rabbit anti-RPN1 (Proteintech; 1:800), rabbit anti-RPN2 (Bethyl Lab; 1:4000), rabbit anti-OST48 (Proteintech; 1:1000), rabbit anti-DAD1 (a gift from Stephen High University of Manchester; 1:2500), rabbit anti-EGFR (sc-03; Santa Cruz Biotechnology; 1:1,000), rabbit anti-phospho (Tyr1173) EGF Receptor (Cell Signaling; 1:1,000), rabbit anti-B1-Integrin (M-106; sc-8978; Santa Cruz Biotechnology; 1:1000), rabbit anti-p21 Waf1/Cip1 (12D1; Cell Signaling; 1:1,000), rabbit anti-Cyclin D1 (Cell Signaling; 1:1,000), mouse anti-β-Actin (8H10D10; Cell Signaling; 1:1,000); rabbit anti-FGF Receptor 1 (D8E4, Cell Signalling; 1:1,000); rabbit anti-phospho FGF Receptor (Tyr653/654) (Cell Signaling; 1:3,000), anti-GADPH (Proteintech; 1:5000), rabbit anti-BIP (Cell Signaling; 1:1,000).

For phospho-protein array analysis, PC9 and A549 cells were cultured in 6-well plates in serum-containing medium and treated with or without 10 μM NGI-1 for 24 hours. The human Phospho-protein array kit (R&D Systems) was used to simultaneously detect the relative site-specific phosphorylation of 43 kinases and 2 related total proteins according to the manufacturer's protocol.

Biotinylation and recovery of cell surface proteins were performed on intact H3255 cell monolayers using EZ-link Sulfo-NHS-SS Biotin (Pierce) and isolated using streptavidin-agarose beads (Sigma-Aldrich). Control or cells treated with 10 μM NGI-1 for 24 h were placed on ice and washed three times with PBS. The cells were incubated with EZ-link

Sulfo-NHS-SS-Biotin at a final concentration of 0.5 mg/ml in PBS for 60 min at 4 °C, followed by 100 mM glycine/PBS wash, and two washes with PBS. Biotinylated cells were scraped into lysis buffer (25 mM Tris-HCl pH 7.4, 10 mM EDTA, 15% glycerol, 0.1% Triton X-100, protease inhibitor tablet (Roche Diagnostics; Indianapolis, IN, USA) and phosphatase inhibitor cocktails 2 and 3 (Sigma-Aldrich)) and agitated on a shaker for 60 min at 4 °C. The cell lysate was centrifuged for 10 min at 14,000 × *g*, and the resulting supernatant was incubated with streptavidin-agarose beads, suspended in lysis buffer, and mixed at 4 °C overnight. The beads were recovered by centrifugation (5,000 × *g* for 15 s) and aliquots of supernatants were taken to represent the unbound, intracellular pool of proteins. Biotinylated proteins were eluted from the beads by heating to 100 °C for 5 min in SDS-PAGE sample buffer before loading onto a 7.5% SDS-PAGE gel for western blot analysis against EGFR or ITB1.

For PNGase digestion 10 μg lysate were digested with peptide N-glycosidase F (PNGase-F, New England Biolabs, Beverly, MA). Specifically, samples were incubated in denaturing buffer (0.5% SDS and 1% β-mercaptoethanol) for 10 min at 100 °C and brought to 50 mM sodium phosphate (pH 7.5) with 1% Nonidet P-40. Then, 1 μl (500 units) of PNGase-F was added and incubated for 1 h at 37 °C. After glycosidase digestion, SDS-PAGE sample buffer was added and incubated at 100 °C for 5 min. Equal amounts of non-digested and digested PNGase-F proteins were subjected to SDS-PAGE and western blot analysis for EGFR.

For Quantitative RT-PCR A549 and PC9 cells were seeded in 6 cm dishes, after NGI-1 treatment total mRNA purification was performed using the RNeasy Mini Kit (QIAGEN) and reverse transcribed into cDNA using iScript™ cDNA Synthesis Kit (BIO-RAD) according to the manufacturer's protocol. The newly synthesized cDNA was amplified using iQ™ SYBR® Green QPCR Supermix (Agilent Technologies) and expression levels of human Cyclin D1 and human GAPDH mRNA were determined using these specific primers: Cyclin D1 forward: 5′-ACCTGAGGAGCCCCAACAA-3′; reverse: 5′-TCTGCTCCTGGCAGGCC-3′. GAPDH forward: 5′-GCTCTCTGCTCCTCCTGTTC-3′; reverse: 5′-ACGACCAAATCCGTTGACTC-3′. The incubation conditions were as follows: 1 cycle at 95°C for 10 min, followed by 40 cycles of 30 sec at 95°C, annealing for 15 sec at 55°C, and extension for 30 sec at 72°C. PCRs for each sample were done in triplicate for all the genes.

Microscopy

For immunofluorescence, H3255 cell lines were grown on glass coverslips to 70% confluence. Cell cultures were washed with PBS and fixed with 4% (w/v) formaldehyde in PBS for 30 min at 37°C. After washing with PBS, cells were permeabilized with 0.1% v/v Triton X-100 in PBS for 10 min, rinsed three times in PBS and treated with 5% w/v bovine serum albumin for 1 h. Cells were then incubated overnight at 4°C with either rabbit anti-EGFR pAb (sc-03; Santa Cruz Biotechnology; 1:2,000), mouse anti-CRT mAb (BD Transduction Laboratories™; 1:1,000) or mouse anti-B1-Integrin mAb (MAB2253; Millipore; 1:500) primary antibodies and for 1 h at room temperature with either Alexa Fluor 543-conjugated goat anti-rabbit IgG or Alexa Fluor 488-conjugated goat anti-mouse IgG (ThermoFisher Scientific; 1:1,000) secondary antibodies. All antibodies were diluted in

PBS containing 5% w/v bovine serum albumin. Nuclei were stained using ToPro3 (Invitrogen). Confocal cellular images were captured with an inverted Zeiss LSM 510 Pascal laser confocal microscope (Carl Zeiss, Jenna, Germany), using a 63/1.4 Plan-Apochromat objective. Quantification of colocalization was performed using Image J Colormap Software.

Glycomics

Cells were surface biotinylated as described above and the lysate was mixed with 2x sample loading buffer containing 50 mM of DTT and boiled for 5 min. The boiled samples were separated by SDS-PAGE (BioRad TGX MiniProtean) for 10 min at 200 V. Each lane of the gel was cut and denatured by incubating with 10 mM of DTT at 56 °C for an hour, alkylated by 55 mM of iodoacetamide for 45 minutes in the dark, and then digested with trypsin at 37 °C overnight. The resulting peptides were extracted, dried and deglycosylated by PNGasF (ProZyme) at 37 °C overnight in the presence of $H_2{}^{18}O$ (Cambridge Isotope Laboratories, Inc.). The deglycosylated peptides were then dried and reconstituted in 0.1% formic acid. The peptides were separated on a 75 μm (I.D.) × 15 cm C18 capillary column (packed in house, YMC GEL ODS-AQ120ÅS-5, Waters) and eluted into the nano-electrospray ion source of an Orbitrap Fusion™ Tribrid™ mass spectrometer (Thermo Fisher Scientific) with a 180-min linear gradient consisting of 0.5–100% solvent B over 150 min at a flow rate of 200 nL/min. The spray voltage was set to 2.2 kV and the temperature of the heated capillary was set to 280 °C. Full MS scans were acquired from m/z 300 to 2000 at 120k resolution, and MS2 scans following collision-induced fragmentation were collected in the ion trap for the most intense ions in the Top-Speed mode within a 3-sec cycle using Fusion instrument software (v1.1, Thermo Fisher Scientific). The raw spectra were searched against the human protein database (UniProt, Oct. 2014) using SEQUEST (Proteome Discoverer 1.4, Thermo Fisher Scientific) with full MS peptide tolerance of 20 ppm and MS2 peptide fragment tolerance of 0.5 Da, and filtered using ProteoIQ (v2.7, Premier Biosoft) to generate a false discovery rate of 1% at protein level and 5% at peptide level for any protein/peptide assignments.

Proliferation assays

Growth rates were determined by CellTiter 96 NonRadioactive Cell Proliferation Assay (Promega; Madison, WI, USA) according to the manufacturer's directions. Briefly, NSCLC cells (2×10^3) untreated or treated with 10 μM NGI-1 or 1 μM Tn, were seeded in triplicates in 96-wells plates and grown in culture medium containing 10% serum. The media was changed with our without new inhibitor every 48h. Cell numbers were estimated after 0, 3, and 5 days by adding MTT (3-(4,5-dimethylthiazol-2-yl)-2,5-diphenyltetrazolium bromide) reagent to the wells 4 h before taking the spectrophotometric reading (absorbance at 570 nm).

Cell cycle distribution

For the assessment of cell cycle distribution, 1×10^6 cells were collected, washed once with ice-cold PBS and fixed in ice-cold 70% ethanol overnight at −20°C. Thereafter, cells were washed twice with PBS and incubated for 30 min at room temperature in 200 μL of Guava Cell Cycle Reagent (Guava Technologies). Cytofluorometric acquisitions were performed on a LSRII cytometer (BD Biosciences). First-line analysis was performed with Flow Jo

software, upon gating of the events characterized by normal forward and side scatter parameters and discrimination of doublets in a FSC-A vs. FSC-H bivariate plot. Approximately 30,000 cells were analyzed per experiment, and the mean value was obtained from 3 independent assays.

Assessment of senescence

Autofluorescence of PC9 and A549 cells untreated or treated with 10 μM NGI-1 for 24 h was characterized by flow cytometry after fixing the cells with 70% ethanol, staining with 4,6-diamino-2-phenyl indole (DAPI) for 30 min. Acquisition was done on a LRSII flow cytometer (BD Biosciences) equipped with green (532 nm) and UV (405nm) lasers and measured by emission at 575 nm after gating with DAPI. Lipofuscin accumulation was detected by confocal laser scanning microscopy using an excitation laser of 405nm with acquired signals from spectrums of yellow 575–620 nm. Morphology changes were explored by differential interference contrast (DIC). Fluorescence and DIC images were captured with a Leica SP5 confocal microscope.

Statistics

Data points are reported as experimental averages and error bars represent standard deviations of at least three independent experiments. No samples were excluded from the analysis. Statistical significance was determined using a two-sided Student's *t* test with Graph-Pad Prism 6 (GraphPad Software Inc.). A P value < 0.05 or less was considered to be statistically significant.

Supplementary Material

Refer to Web version on PubMed Central for supplementary material.

Acknowledgments

This work was funded by R03DA033178, R01CA172391, and in part by a Research Scholar Grant from the American Cancer Society (JNC) and by RO1GM43768 (RG) and RO1GM038545 (MAL). Additional funding was provided by the NIH-MLPCN program U54HG005031 (Kansas University) and U54HG005032 (Broad Institute). The Mass Spectrometry work was supported by NIH grant P41GM103490.

References

1. Zielinska DF, Gnad F, Wisniewski JR, Mann M. Precision mapping of an in vivo N-glycoproteome reveals rigid topological and sequence constraints. Cell. 2010; 141:897–907. [PubMed: 20510933]
2. Freeze HH. Genetic defects in the human glycome. Nat Rev Genet. 2006; 7:537–51. [PubMed: 16755287]
3. Lehrman MA. Teaching dolichol-linked oligosaccharides more tricks with alternatives to metabolic radiolabeling. Glycobiology. 2007; 17:75R–85R.
4. Takatsuki A, Arima K, Tamura G. Tunicamycin, a new antibiotic. I. Isolation and characterization of tunicamycin. J Antibiot (Tokyo). 1971; 24:215–23. [PubMed: 5572750]
5. Helenius J, et al. Translocation of lipid-linked oligosaccharides across the ER membrane requires Rft1 protein. Nature. 2002; 415:447–50. [PubMed: 11807558]
6. Frank CG, Sanyal S, Rush JS, Waechter CJ, Menon AK. Does Rft1 flip an N-glycan lipid precursor? Nature. 2008; 454:E3–4. discussion E4–5. [PubMed: 18668045]

7. Jelk J, et al. Glycoprotein biosynthesis in a eukaryote lacking the membrane protein Rft1. J Biol Chem. 2013; 288:20616–23. [PubMed: 23720757]
8. Aebi M. N-linked protein glycosylation in the ER. Biochim Biophys Acta. 2013; 1833:2430–7. [PubMed: 23583305]
9. Kelleher DJ, Gilmore R. An evolving view of the eukaryotic oligosaccharyltransferase. Glycobiology. 2006; 16:47R–62R.
10. Pfeffer S, et al. Structure of the mammalian oligosaccharyl-transferase complex in the native ER protein translocon. Nat Commun. 2014; 5:3072. [PubMed: 24407213]
11. Reiss G, te Heesen S, Gilmore R, Zufferey R, Aebi M. A specific screen for oligosaccharyltransferase mutations identifies the 9 kDa OST5 protein required for optimal activity in vivo and in vitro. EMBO J. 1997; 16:1164–72. [PubMed: 9135133]
12. Zufferey R, et al. STT3, a highly conserved protein required for yeast oligosaccharyl transferase activity in vivo. EMBO J. 1995; 14:4949–60. [PubMed: 7588624]
13. Schwarz F, Aebi M. Mechanisms and principles of N-linked protein glycosylation. Curr Opin Struct Biol. 2011; 21:576–82. [PubMed: 21978957]
14. Ruiz-Canada C, Kelleher DJ, Gilmore R. Cotranslational and posttranslational N-glycosylation of polypeptides by distinct mammalian OST isoforms. Cell. 2009; 136:272–83. [PubMed: 19167329]
15. Shrimal S, Gilmore R. Glycosylation of closely spaced acceptor sites in human glycoproteins. J Cell Sci. 2013; 126:5513–23. [PubMed: 24105266]
16. Cherepanova NA, Shrimal S, Gilmore R. Oxidoreductase activity is necessary for N-glycosylation of cysteine-proximal acceptor sites in glycoproteins. J Cell Biol. 2014; 206:525–39. [PubMed: 25135935]
17. Roboti P, High S. The oligosaccharyltransferase subunits OST48, DAD1 and KCP2 function as ubiquitous and selective modulators of mammalian N-glycosylation. J Cell Sci. 2012; 125:3474–84. [PubMed: 22467853]
18. Blomen VA, et al. Gene essentiality and synthetic lethality in haploid human cells. Science. 2015; 350:1092–6. [PubMed: 26472760]
19. Freeze HH, Aebi M. Altered glycan structures: the molecular basis of congenital disorders of glycosylation. Curr Opin Struct Biol. 2005; 15:490–8. [PubMed: 16154350]
20. Contessa JN, et al. Molecular imaging of N-linked glycosylation suggests glycan biosynthesis is a novel target for cancer therapy. Clin Cancer Res. 2010; 16:3205–14. [PubMed: 20413434]
21. Dennis JW, Nabi IR, Demetriou M. Metabolism, cell surface organization, and disease. Cell. 2009; 139:1229–41. [PubMed: 20064370]
22. Croci DO, et al. Glycosylation-dependent lectin-receptor interactions preserve angiogenesis in anti-VEGF refractory tumors. Cell. 2014; 156:744–58. [PubMed: 24529377]
23. Weinstein IB, Joe A. Oncogene addiction. Cancer Res. 2008; 68:3077–80. discussion 3080. [PubMed: 18451130]
24. Kellenberger C, Hendrickson TL, Imperiali B. Structural and functional analysis of peptidyl oligosaccharyl transferase inhibitors. Biochemistry. 1997; 36:12554–9. [PubMed: 9376360]
25. Weerapana E, Imperiali B. Peptides to peptidomimetics: towards the design and synthesis of bioavailable inhibitors of oligosaccharyl transferase. Org Biomol Chem. 2003; 1:93–9. [PubMed: 12929394]
26. Bennett DC, et al. High-throughput screening identifies aclacinomycin as a radiosensitizer of EGFR-mutant non-small cell lung cancer. Transl Oncol. 2013; 6:382–91. [PubMed: 23730419]
27. Baell JB, Holloway GA. New substructure filters for removal of pan assay interference compounds (PAINS) from screening libraries and for their exclusion in bioassays. J Med Chem. 2010; 53:2719–40. [PubMed: 20131845]
28. Auld DS, et al. Molecular basis for the high-affinity binding and stabilization of firefly luciferase by PTC124. Proc Natl Acad Sci U S A. 2010; 107:4878–83. [PubMed: 20194791]
29. Maeda Y, Tomita S, Watanabe R, Ohishi K, Kinoshita T. DPM2 regulates biosynthesis of dolichol phosphate-mannose in mammalian cells: correct subcellular localization and stabilization of DPM1, and binding of dolichol phosphate. EMBO J. 1998; 17:4920–9. [PubMed: 9724629]

30. Anand M, et al. Requirement of the Lec35 gene for all known classes of monosaccharide-P-dolichol-dependent glycosyltransferase reactions in mammals. Mol Biol Cell. 2001; 12:487–501. [PubMed: 11179430]
31. Mohorko E, et al. Structural basis of substrate specificity of human oligosaccharyl transferase subunit N33/Tusc3 and its role in regulating protein N-glycosylation. Structure. 2014; 22:590–601. [PubMed: 24685145]
32. Kelleher DJ, Karaoglu D, Gilmore R. Large-scale isolation of dolichol-linked oligosaccharides with homogeneous oligosaccharide structures: determination of steady-state dolichol-linked oligosaccharide compositions. Glycobiology. 2001; 11:321–33. [PubMed: 11358881]
33. Shrimal S, Trueman SF, Gilmore R. Extreme C-terminal sites are posttranslocationally glycosylated by the STT3B isoform of the OST. J Cell Biol. 2013; 201:81–95. [PubMed: 23530066]
34. Jafari R, et al. The cellular thermal shift assay for evaluating drug target interactions in cells. Nat Protoc. 2014; 9:2100–22. [PubMed: 25101824]
35. Paez JG, et al. EGFR mutations in lung cancer: correlation with clinical response to gefitinib therapy. Science. 2004; 304:1497–500. [PubMed: 15118125]
36. Pao W, et al. EGF receptor gene mutations are common in lung cancers from “never smokers” and are associated with sensitivity of tumors to gefitinib and erlotinib. Proc Natl Acad Sci U S A. 2004; 101:13306–11. [PubMed: 15329413]
37. Sordella R, Bell DW, Haber DA, Settleman J. Gefitinib-sensitizing EGFR mutations in lung cancer activate anti-apoptotic pathways. Science. 2004; 305:1163–7. [PubMed: 15284455]
38. Weiss J, et al. Frequent and focal FGFR1 amplification associates with therapeutically tractable FGFR1 dependency in squamous cell lung cancer. Sci Transl Med. 2010; 2:62ra93.
39. Schneider A, et al. Successful prenatal mannose treatment for congenital disorder of glycosylation-Ia in mice. Nat Med. 2012; 18:71–3.
40. Leung EL, et al. SRC promotes survival and invasion of lung cancers with epidermal growth factor receptor abnormalities and is a potential candidate for molecular-targeted therapy. Mol Cancer Res. 2009; 7:923–32. [PubMed: 19491201]
41. Shimamura T, Lowell AM, Engelman JA, Shapiro GI. Epidermal growth factor receptors harboring kinase domain mutations associate with the heat shock protein 90 chaperone and are destabilized following exposure to geldanamycins. Cancer Res. 2005; 65:6401–8. [PubMed: 16024644]
42. Kobayashi S, et al. Transcriptional profiling identifies cyclin D1 as a critical downstream effector of mutant epidermal growth factor receptor signaling. Cancer Res. 2006; 66:11389–98. [PubMed: 17145885]
43. Arrowsmith CH, et al. The promise and peril of chemical probes. Nat Chem Biol. 2015; 11:536–41. [PubMed: 26196764]
44. Gao N, Lehrman MA. Analyses of dolichol pyrophosphate-linked oligosaccharides in cell cultures and tissues by fluorophore-assisted carbohydrate electrophoresis. Glycobiology. 2002; 12:353–60. [PubMed: 12070078]
45. Gao N, Shang J, Lehrman MA. Analysis of glycosylation in CDG-Ia fibroblasts by fluorophore-assisted carbohydrate electrophoresis: implications for extracellular glucose and intracellular mannose 6-phosphate. J Biol Chem. 2005; 280:17901–9. [PubMed: 15708848]

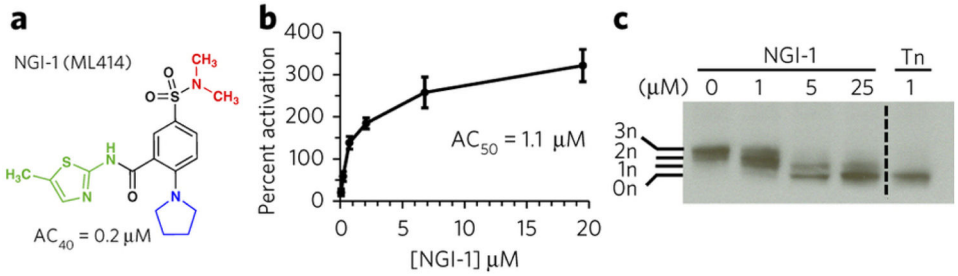

Figure 1. HTS for inhibitors of N-linked glycosylation

a. Structure activity relationships (SAR) for the aminobenzamidosulfonamide series. The AC_{40} values for each analog are derived from the SmartFit algorithm for replicate experiments (n=2–6; see suppl. Tables 1–3) and are reported for comparison. **b.** Dose response activation of D54 ERLucT cells, maximum activation using 20 μM NGI-1 was used to calculate AC_{50}. Results are the average of n=4 experiments. **c.** Representative dose response inhibition of luciferase glycosylation by western blot (n=3) (Suppl. Fig. 9a). Glycoforms are identified as 0–3n.

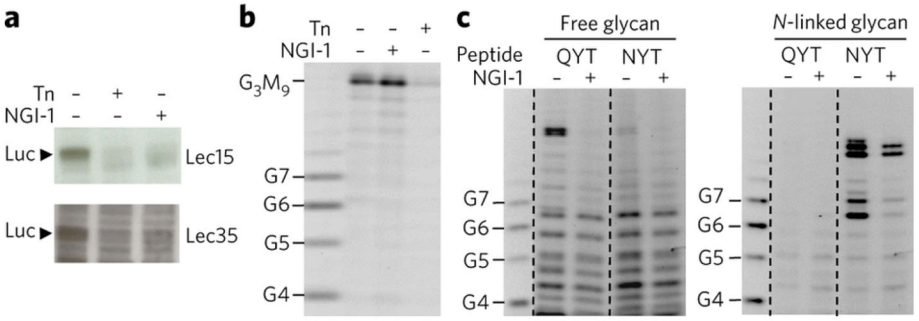

Figure 2. NGI-1 blocks LLO transfer and hydrolysis

a. Western blots of glycosylated luciferase in CHO-Lec15 and CHO-Lec35 cells with stable expression of ER-LucT after 24 h treatment with 1 μM tunicamycin (Tn) and 10 μM NGI-1 (Suppl. Fig. 9b). **b.** Representative FACE analysis of LLOs after NGI-1 or Tn treatment in wild type CHO cells (n=3). G_3M_9 indicates the size of the mature LLO containing 3 glucose and 9 mannose carbohydrate units. **c.** Representative FACE analysis of free glycans (n=2) or cleaved N-linked glycans (n=2) from Streptolysin-O permeabilized CHO cells incubated with a control peptide (QYT) or an N-linked glycosylation consensus acceptor peptide (NYT). The effects of NGI-1 (5 μM) on free glycans (left panel) and N-linked glycans cleaved from glycopeptides with PNGase (right panel) are shown. Carbohydrate size is indicated with glucose markers (G4–G7).

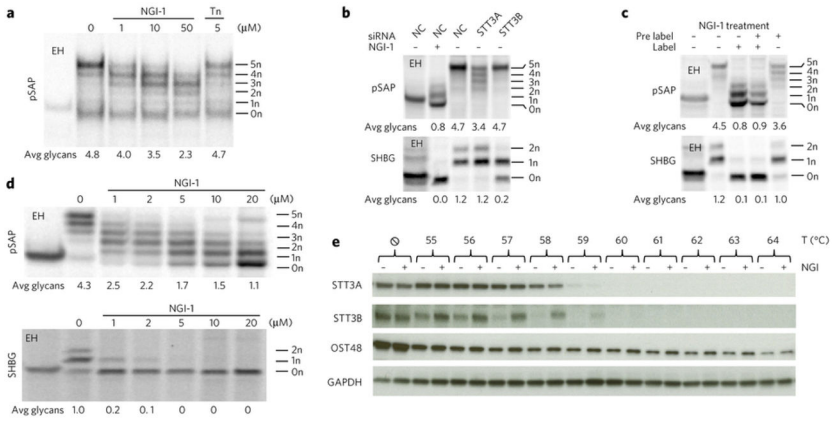

Figure 3. NGI-1 blocks OST function

a. Cell free inhibition of the OST using ^{35}S metabolic labeling in rabbit reticulocyte lysates supplemented with canine pancreas rough microsomes. Saposin-DDK-His$_6$ mRNA was translated for 60 min in the presence of NGI-1 or Tn. **b–d**. ^{35}S labeling of pSAP and SHBG in HeLa cells after 10 μM NGI-1 treatment. **b.** Results from NGI-1 are compared to siRNA knockdown of STT3A or STT3B. Glycoforms are represented by 0–5n and 0–2n, respectively, and the average number of glycans per sample is reported for each condition. NC= non-coding siRNA, EH= endoglycosidase H treated. **c.** HeLa cells were treated with or without NGI-1 for 24 h prior to addition of the ^{35}S label, during labeling, or both to demonstrate reversibility of the inhibitor. **d.** Dose response of NGI-1 effect on pSAP and SHBG glycosylation expressed in HEK293 cells **e.** CETSA for subunits of the OST in 293T cells treated with and without 100 μM NGI-1 for 30 min (Suppl. Fig. 9c). The denotes no thermal treatment. Each panel is representative of two independent experiments.

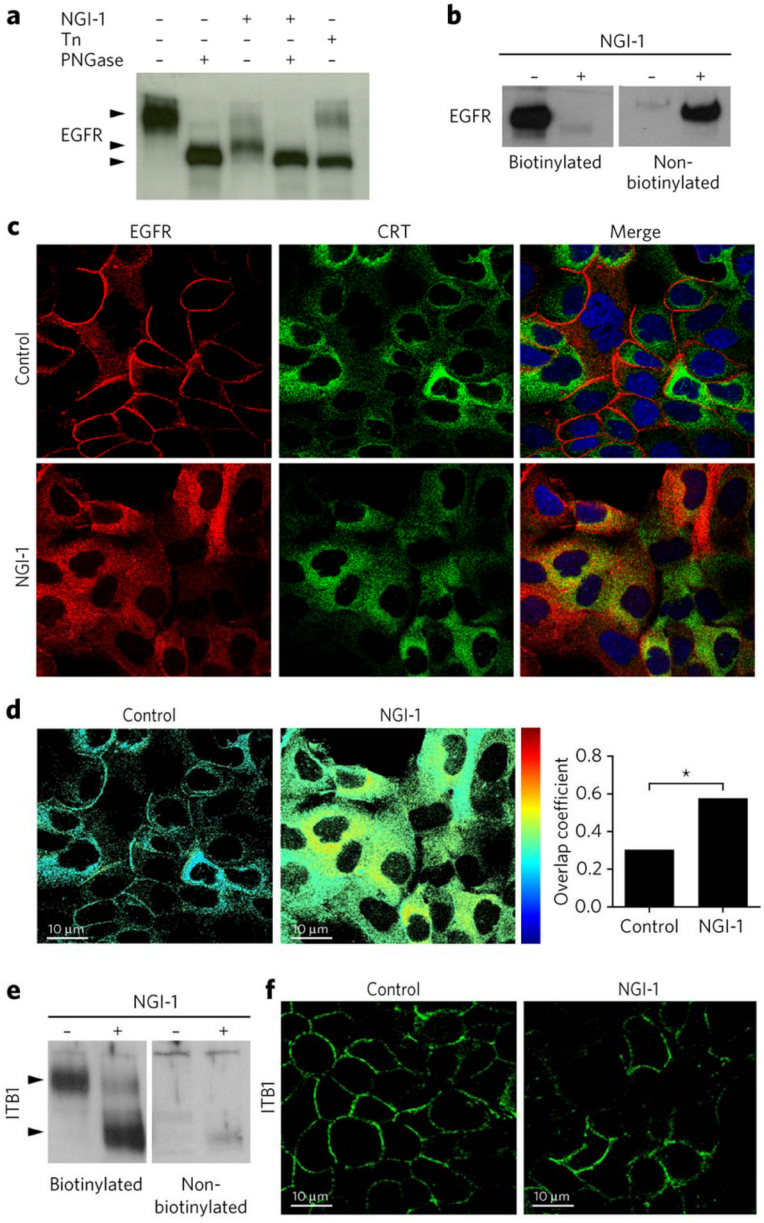

Figure 4. NGI-1 disrupts EGFR glycosylation and cell surface expression

a. Western blot of EGFR treated with 10μM NGI-1 for 24h; molecular size shifts are compared to PNGase digestion and tunicamycin (Tn) treatment (Suppl. Fig. 9d). **b.** Surface protein biotinylation and streptavidin precipitation to compare EGFR localization in plasma membrane and cytoplasmic fractions (Suppl. Fig. 9e). **c.** Confocal microscopy and immunofluorescence of EGFR protein (red) and CRT (green) with nuclear ToPro3 counterstain (cyan). **d.** Quantification of EGFR and CRT colocalization; color scale displays positive (red/yellow) or negative (blue/green) correlations. Colocalization was calculated by averaging the data obtained from 10 different fields of two independent experiments. Data are represented as mean ± s.d., *p* values were determined using two-tailed *t*-tests. $*P < 0.05$. ITB1 localization after 10μM NGI-1 for 48 h analyzed by (**e.**) surface biotinylation (Suppl.

Fig. 9f) (**f.**) confocal microscopy (green). Results for each panel are representative of at least three independent experiments unless otherwise noted. Scale bars, 10 μm.

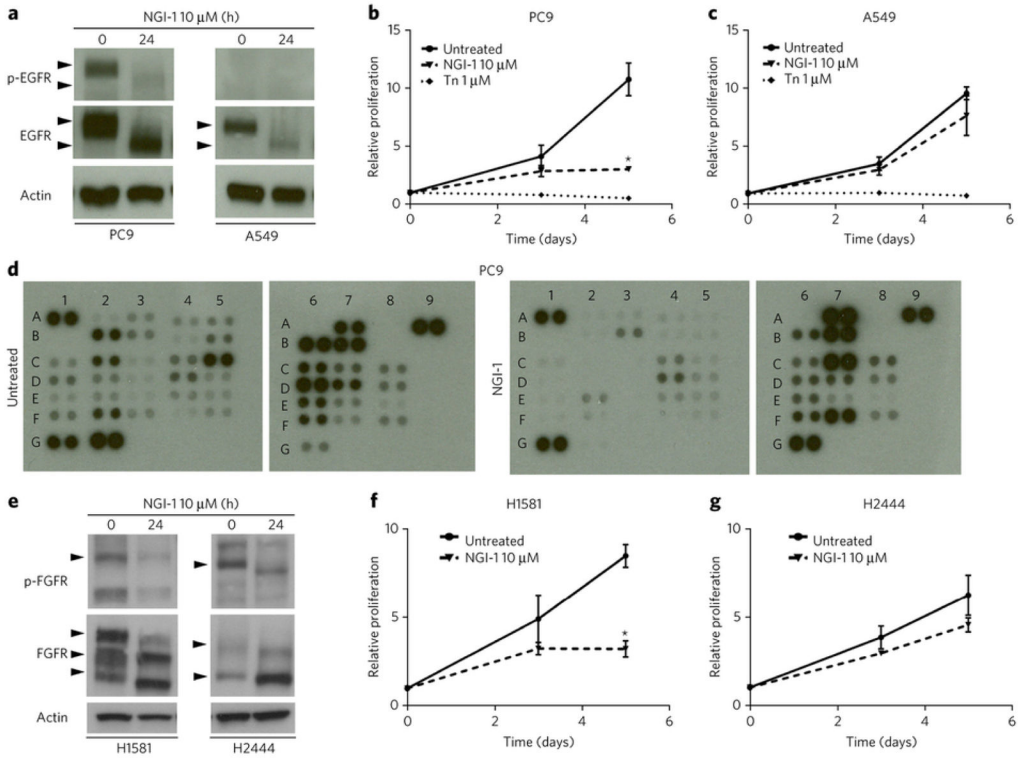

Figure 5. NGI-1 blocks RTK driven proliferation

a. EGFR phosphorylation (Y1173) and gel mobility in PC9 and A549 NSCLC cells after 10μM NGI-1 treatment for 24 h (Suppl. Fig. 9g). Arrows indicate changes in glycoforms. **b–c.** Fold proliferation measured by MTT over 5 days with 10μM NGI-1 or 1μM tunicamycin treatment. **d.** Phospho-protein array profiles of PC9 cells with or without 10μM NGI-1 for 24 h. Duplicate phosphoprotein intensities are labeled with a coordinate system (e.g. B2 represents EGFR phosphorylation; see suppl. Fig. 6b for phospho-protein quantification). NGI-1 has global effects on signaling protein phosphorylation in PC9 cells (compare (d.) left and right panels) but not A549 cells (compare suppl. Fig. 6a.) left and right panels) **e.** FGFR phosphorylation (Y653/654) and gel mobility for H1581 and H2444 NSCLC cell lines (Suppl. Fig. 9h). **f–g**. MTT assays for H1581 and H2444 cells treated with 10μM NGI-1 for 5 d. Data are represented as mean ± s.d., $n = 3$. P values were determined using two-tailed t-tests. $*P < 0.001$.

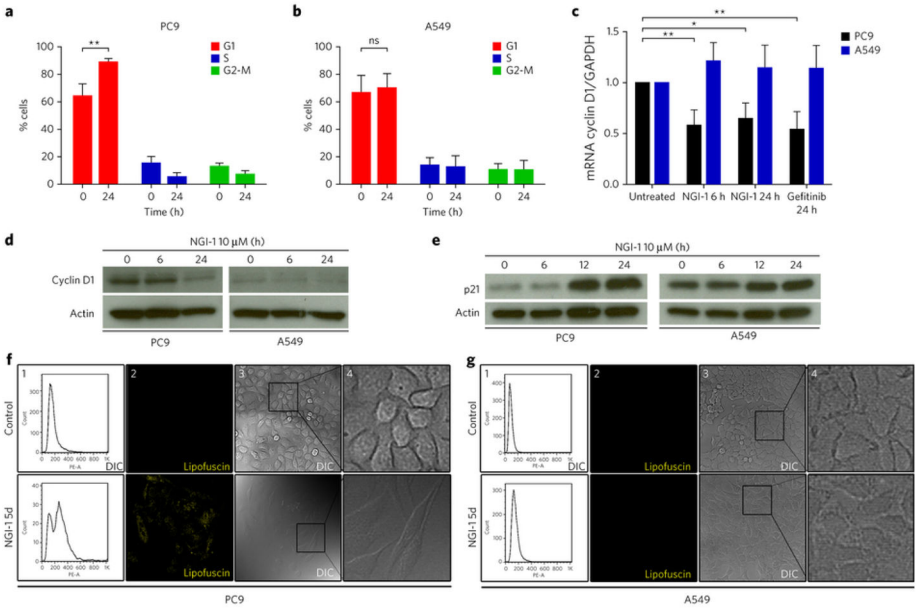

Figure 6. NGI-1 induces G1 arrest and senescence in EGFR addicted tumor cells

a–b. Flow cytometry and cell cycle distribution of PC9 and A549 cells after NGI-1 treatment for 24 h. Data are represented as mean ± s.d., $n = 3$. P values were determined using two-tailed t-tests. $^{**}P < 0.01$, ns, not significant. **c.** mRNA levels of cyclin D1 gene were determined by qRT-PCR using SYBR Green and normalized to *GAPDH*. Data are represented as mean ± s.d., $n = 4$. P values were determined using two-tailed t-tests. $^{**}P < 0.05$ or $^{**}P < 0.01$. Representative western blot for **d.** Cyclin D1 protein (n=3), and (Suppl. Fig. 9i) **e.** p21 induction (n=3) in PC9 and A549 cells (Suppl. Fig. 9j). **f–g.** Senescence determined by flow cytometry analysis of autofluorescence at 575 nm (panel 1; n=4), confocal laser scanning microscopy using 405/575–620 nm excitation and emission spectra (panel 2; n=3), and morphology changes (panel 3,4; n=3).